Research Article | Vol. 10, No. 11 / 1 November 2019 / Biomedical Optics Express 5650
Biomedical Optics EXPRESS

Characterization of oviduct ciliary beat frequency using real time phase resolved Doppler spectrally encoded interferometric microscopy

YOUMIN HE,[1,2] YUEQIAO QU,[1,2] JOSEPH C. JING,[1] AND ZHONGPING CHEN[1,*]

[1] *Beckman Laser Institute, Department of Biomedical Engineering, University of California, Irvine, 1002 Health Sciences Road East, Irvine, CA 92612, USA*
[2] *First two authors contributed equally to this study*
[*] *z2chen@uci.edu*

Abstract: Ciliary activity, characterized by the coordinated beating of ciliary cells, generates the primary driving force for oviduct tubal transport, which is an essential physiological process for successful pregnancies. Malfunction of the cilium in the fallopian tube, or oviduct, may increase the risk of infertility and tubal pregnancy that can result in maternal death. While many ex-vivo studies have been carried out using bright field microscopy, this technique is not feasible for the in-vivo investigation of oviduct ciliary beating frequency (CBF). Optical coherence tomography (OCT) has been able to provide in-vivo CBF imaging in a mouse model, but its resolution may be insufficient to resolve the spatial and temporal features of the cilium. Our group has recently developed the phase resolved Doppler (PRD) OCT method to visualize ciliary strokes at ultra-high displacement sensitivity. However, the cross-sectional field of view (FOV) may not be ideal for visualizing the surface dynamics of ciliated tissue. In this study, we report on the development of phase resolved Doppler spectrally encoded interferometric microscopy (PRD-SEIM) to visualize the oviduct ciliary activity within an en face FOV. This novel real time imaging system offers micrometer spatial resolution, sub-nanometer displacement sensitivity, and the potential for in-vivo endoscopic adaptation. The feasibility of the approach has been validated through ex-vivo experiments where the porcine oviduct CBF has been measured across different temperature conditions and the application of a drug. CBF ranging from 8 to 12 Hz have been observed at different temperatures, while administration of lidocaine decreased the CBF and deactivated the motile cilia. This study will serve as a stepping stone to in-vivo oviduct ciliary endoscopy and future clinical translations.

1. Introduction

Tubal transport is an essential process for successful spontaneous pregnancy by controlling the interaction between gametes as well as delivering the fertilized ovum to the uterus for implantation [1–3]. Dysfunctions in tubal transport, such as failure to capture the oocytes or transport the ovum, can induce infertility or life-threatening ectopic pregnancy [4–6]. Within the oviduct, the two major effectors for tubal transport include the smooth muscle contractions and the coordinated ciliary beats [7,8]. Pilot studies further indicated that ciliary activity plays a dominant role in the transportation of the fertilized ovum [9,10]. Particularly, the synchronized beating of the cilia generates the driving force to move the fluid as well as the ovum through the oviduct [6]. Therefore, it is of great significance to study the frequency and synchronicity of oviduct ciliary activity to better understand the etiology of fallopian tube related ectopic pregnancy or infertility.

Over the past several years, bright field microscopy has been the core technique to visualize the ciliary activity and measure the CBF using the light fluctuations induced by ciliary beats [11–20].

#367558 https://doi.org/10.1364/BOE.10.005650
Journal © 2019 Received 14 May 2019; revised 31 Jul 2019; accepted 4 Aug 2019; published 11 Oct 2019

Biomedical Optics EXPRESS

However, bright field microscopy is currently incapable to investigate the ciliary activity of in-vivo tissues due to the tradeoff between the size and resolution of its endoscope. The resolution of white light endoscopy relies on the number of fiber bundles or the pixel size of digital cameras, and it is thereby difficult to achieve micron scale resolution with a sub-millimeter probe diameter [21]. Recently, high resolution optical coherence tomography (OCT) has been utilized to assess the in-vivo ciliary activity of oviduct and airway tissues [22–26]. The depth resolved imaging capabilities of OCT allows for access to the inner cavity of the fallopian tube through the open abdominal cavity, and the CBF is measured by analyzing the intensity fluctuations at ciliated sites [22,23]. Although endoscopic OCT has the potential for in-vivo oviduct CBF imaging, it is still insufficient to visualize the complex patterns and synchronicity of ciliary behavior due to the limited resolution in resolving the ciliary strokes on the micron level [27,28].

The phase resolved Doppler (PRD) method can provide sub-nanometer displacement sensitivity for interferometric imaging and has been utilized for many applications that require ultra-sensitive movement detection [29–37]. Therefore, a PRD-enhanced technique will be a better candidate for ciliary motion detection. In particular, our group has recently developed a PRD-OCT system for the nanometer-scale visualization of the ciliary beating cycles and validated the feasibility of using the PRD method to investigate the spatial and temporal behaviors of the cilium [27]. In addition, since ciliary activity naturally occurs on the surface of the tissue, cross-sectional imaging techniques, such as OCT, may not provide the most suitable field of view (FOV). More specifically, a cross-sectional image may not encompass the complete ciliary stroke and much of its FOV will be occupied by the non-ciliated regions. Current OCT speed is not fast enough to generate large enface FOV to characterize the complex pattern and synchronization of cilia beating dynamics.

To address these issues, we developed phase resolved Doppler spectrally encoded interferometric microscopy (PRD-SEIM) to visualize the real time surface dynamics of the oviduct. Spectrally encoded interferometry (SEI) allows for en face imaging and will thereby provide a more suitable FOV, compared to that of OCT, to visualize the surface activities of ciliated tissue [38,39]. In addition, endoscopic SEI is capable of high resolution imaging with a probe diameter comparable to that of OCT, and thereby has the potential for in-vivo non-invasive oviduct imaging [40]. Lastly, the PRD method enables nanometer detection of ciliary displacement and allows for clear visualization of the spatial behavior of the active cilium [29,41]. Pilot studies have demonstrated Doppler SEI imaging using a continuous wave laser [42–44], while we have optimized the design by using a high speed swept source laser as the light source. Recent studies have suggested that swept source based low coherence interferometry can provide faster imaging speed, more robustness against fringe washout, comparable sensitivity and resolution when compared to the interferometry based on a continuous wave laser [45–49]. Driven by an akinetic swept source laser, the PRD-SEIM system can achieve 94 frames per second (fps) imaging over an en face area of up to 1 mm^2. To the best of our knowledge, this is the first study that utilizes the PRD-SEIM technique to investigate the oviduct ciliary activity and is expected to provide a powerful tool for in-vivo endoscopic imaging in the future.

2. Methods

2.1. Spectrally encoded microscopy system design

Figure 1 shows a schematic diagram of the SEIM system driven by a swept-source laser. An optical coupler (OC1) splits the light energy, transferring 20% to the reference arm and 80% to the sample arm. In the reference arm, a mirror (M2) reflects the light back to a second optical coupler (OC2.) In the sample arm, the diffraction grating (GR) separates the different wavelengths of light into a line with each complete laser sweep and acts as the fast axis scanner. For the purpose of en face imaging, the system utilizes a Galvanometer mirror (G1) to drive the scan in the slow axis. Lenses L1-L4 act as a relay to center the light on the Galvanometer mirror and the back

Biomedical Optics EXPRESS

focal point of the objective, ensuring that the scan region is entirely flat on the sample. The back scattered light from the sample will interfere with the reflected light from the reference arm via the second coupler (OC2), generating an interferogram that is then detected and digitized by the balanced detector and PC respectively. The center wavelength of the system is 1.3 um, the fast axis scan rate is 400 MHz, as determined by the rate that the laser emits each wave number, and the slow axis scan rate is 100 kHz, as determined by the laser repetition rate. The optical system allows for a lateral resolution of 1.2 um, axial displacement sensitivity of 0.155 nm, and a FOV of approximately 480×750 um. The axial displacement sensitivity was measured using the self-interference signal from a 1mm thick microscope slide based on the method described in [50]. We have recently evaluated the phase variation of the interference signal and found out that the standard deviation of the phase variation, $\Delta\phi(t)$, is approximately 2 mrad, corresponding to a displacement error of ~0.155nm by using the Doppler equation as shown by eq1.

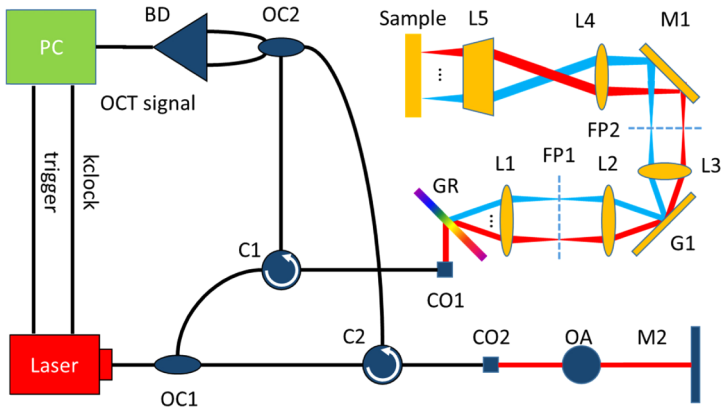

Fig. 1. System setup for spectrally encoded interferometric microscopy. OC1-OC2: optical coupler, C1-C2: circulator, CO1-CO2: collimator, OA: optical attenuator, M1-M2: mirror, BD: balanced detector, GR: diffraction grating (1145 lines per mm), L1-L4: achromatic lens, L5: 0.4 NA objective lens, G1: galvanometer, FP: focal plane

2.2. *Ex vivo tissue preparation*

Porcine oviduct samples were harvested form freshly euthanized female Yorkshire porcines. After dissection, the sample was placed in a sterilized container with Hanks Balanced Salt Solution (HBSS) at a room temperature of around 23 °C. The ampulla portion of the fallopian tube was surgically extracted, cut along the long axis, and laid open for optical access. The sample was then pinned down on a silicone-lined petri dish for stabilization during imaging, and submerged with HBSS to maintain essential nutrients and ions for ciliary beating. Lastly, the petri dish was placed on a heating plate for temperature regulation, and the optical detection beam was then focused on the inner lining of the ampulla. During the temperature-sensitive experiments, the heating plate is used to control the temperature and images were taken approximately 2 minutes after the temperature has stabilized as monitored by a near infrared thermometer. For the experiment with lidocaine administration, we added 2% lidocaine to the petri dish containing the HBSS and the sample, and images were taken before and 5 minutes after the drug application.

2.3. *Data processing*

According to the previous publication, the phase resolved Doppler (PRD) method is able to visualize the ciliary motion by analyzing the interferometric data [27]. Specifically, the PRD algorithm defines a linear relationship between the ciliary displacement, Δd, and the temporal

Biomedical Optics EXPRESS

phase change, $\Delta\varphi$, of the interferogram. Equations 1 and 2 demonstrate the PRD theory to estimate sample displacements within one fast scan using the digitized SEIM signal.

$$\Delta d(x,\ t) = \frac{\lambda}{4\pi n} * \Delta\varphi(x,\ t) \tag{1}$$

$$\Delta\varphi(x,\ t) = \varphi(x,\ t + \Delta t) - \Delta\varphi(x,\ t) \tag{2}$$

Where n denotes the refractive index, λ denotes the wavelength, x denotes the fast axis, and t denotes the time. Since SEIM splits wavelengths in the fast scan axis, λ corresponds to the fast axis, x. In this study, we measure the inter-frame displacement and therefore the frame rate determines the sampling interval, Δt. To fully resolve the periodical activities of the cilia, the system oversamples the ciliated tissue at 94 fps, which allows for frequency measurements of up to 47 Hz.

Using the concepts of PRD, the complete processing algorithm follows the flow chart shown in Fig. 2. First, the algorithm utilizes the Hilbert Transform to generate the analytical form of the raw SEIM signal, from which the phase term can be extracted. Second, the PRD algorithm converts the phase value to the displacement information using Eq. 1. By performing these two steps on every spatial position, algorithm can eventually map out the en face displacement images over time. Using a Cooley-Tukey and Bluestein fast Fourier Transform (FFT) to implement the Hilbert transform, the total time complexity to obtain an en face displacement map is $O(MN\log_2 N)$, where M is the number of A-lines per image and N is the number of points per A-line. One method to increase the processing speed is to parallelize the algorithm, which can reduce the run time by a factor of MN in theory. First, the parallelized algorithm processes all the A-lines simultaneously, accelerating by a factor of M. Second. It is possible to break down most steps of each A-line processing into N parallelizable sub-problems, so that the resulting total reduction in run time will be approximately MN. In this study, we utilized two GPUs (graphic processing unit) to parallelize the algorithm and achieved real time displacement imaging of up to 200 fps with 1000×2048 pixels.

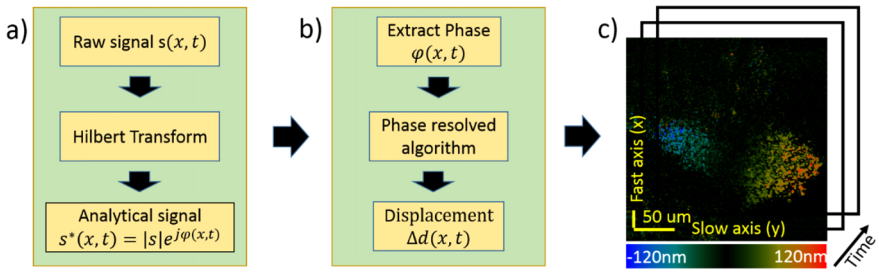

Fig. 2. Processing algorithm for PRD-SS-SEIM system. a) Conversion of the raw signal to its analytical form using the Hilbert Transform. b) Extraction of the phase term and calculation of the displacement using the phase resolved Doppler algorithm. c) En face displacement images of a ciliated area over time.

The en face displacement images enable analysis on both the pattern and the frequency of cilia beats. The spatial and temporal pattern can be visualized directly from the temporal en face (Fig. 3(a)) and M-mode images (Fig. 3(b)). Figure 3(c) shows the displacement at a single ciliated site, and Fig. 3(d) is the corresponding Fourier domain analysis showing the CBF at the peak of the plot. By performing temporal Fourier domain over the entire field of view, the spatial CBF can be visualized as demonstrated by Fig. 3(e). Additionally, the histogram analysis in Fig. 3(f) can help visualize the mean and standard deviation of the spatial CBF image.

Biomedical Optics EXPRESS

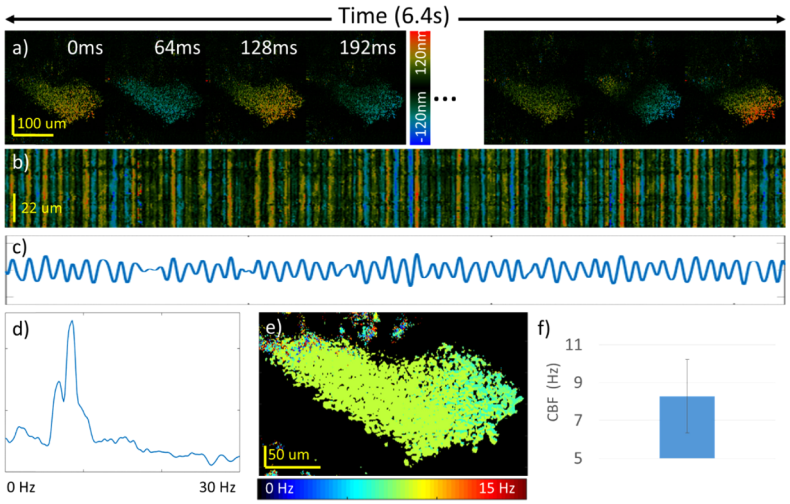

Fig. 3. Analysis method for spatial ciliary activity. a) Temporal displacement images showing periodical ciliary activity. b) M-mode displacement of a single fast scan. c) Quantitative displacement at a single location. d) Spectrum of the displacement showing the ciliary beat frequency (CBF) at its peak. e) Spatial mapping of CBF. f) Histogram of the CBF.

3. Results

In order to visualize and register the spatial and temporal ciliary movement, en face images have been taken continuously at the surface of the ciliated layer. By integrating the PRD algorithm, the system can provide high contrast between actively moving cilia and the static background. The GPU accelerated imaging program further enables instant feedback (detection of active cilia), which allows for real time positioning and alignment over the entire surface of the sample. During the imaging, we have observed both synchronized and unsynchronized ciliary motion. For studying the spatial CBF, we focus the study only on the areas with synchronized ciliary activity.

3.1. Spatially mapped CBF vs. temperature

To understand the influence of temperature on the oviduct cilia, we have performed SEIM imaging on the oviduct sample with varying temperature conditions at 23 °C, 26 °C, 29 °C, and 32°C, respectively. The preparation of the sample follows the procedure as described in the methods section and en face displacement images was taken at a region of synchronized ciliary activity for a period of 6.4 s. Figure 4 shows the time-series displacement images at the same region under different temperature conditions, and the colors correspond to the amplitude and direction of the displacement, where black represents minimal displacement while red and blue show opposite displacement directions.

Based on the sampling theory, the resolution of the frequency is proportional to the reciprocal of the sampling time. In order to accurately measure the CBF and differentiate the subtle CBF changes over temperature, the en face images were continuously acquired at 94 Hz for 6.4 second, providing a frequency resolution of approximately 0.1 Hz. The M-mode images clearly visualize the complete ciliary beating cycle, demonstrating the sufficiency of the sampling rate. The temporal profile in Fig. 5(a) is generated by vertically averaging all the M-mode images. Although the magnitude of the ciliary beats fluctuates in the temporal profile, the duration of each cycle seems to be consistent at each temperature. Therefore, it is feasible to use the Fourier

Biomedical Optics EXPRESS

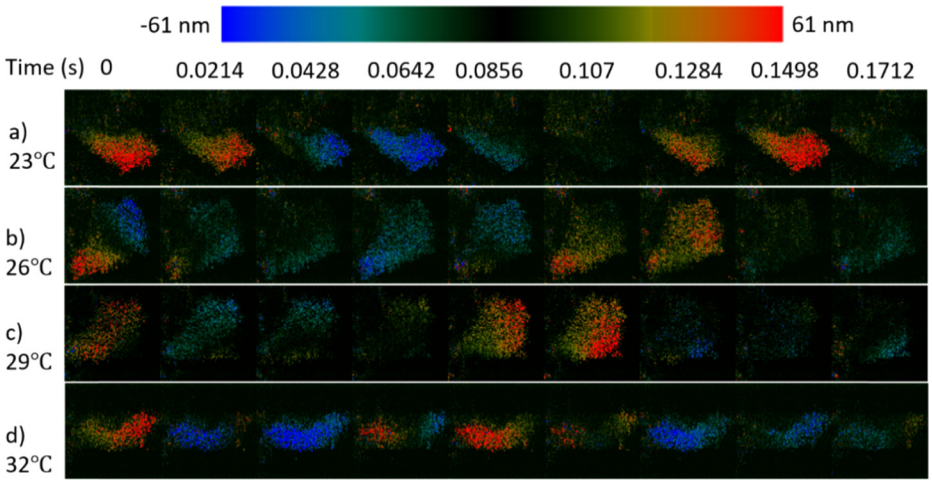

Fig. 4. Periodical Ciliary activity at different temperature. a-d) Coordinated ciliary beating cycle from 0 to 0.17 s at 23 °C, 26 °C, 29 °C, and 33 °C respectively (Visualization 1).

transform to analyze the beating frequency. The Fourier transform was then performed on the temporal profile, and the CBF can be identified by the peak. The value of the CBF has been calculated to range from 8.5Hz to 12Hz with increasing temperatures.

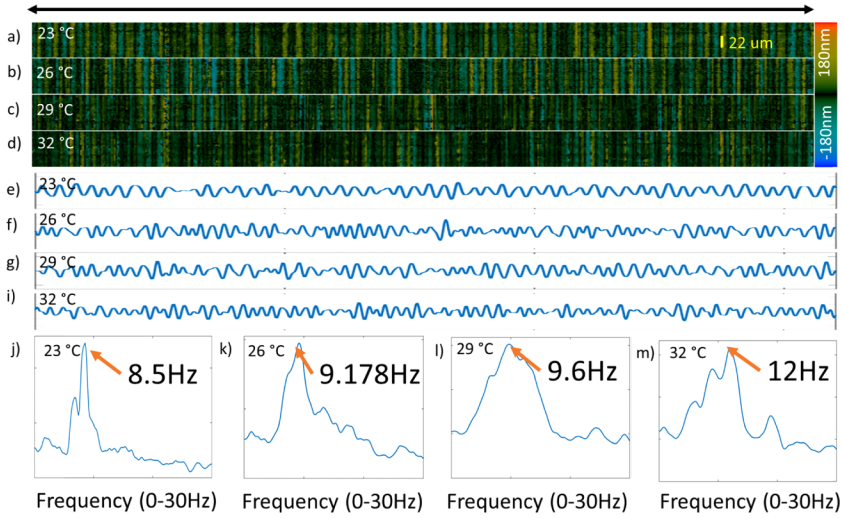

Fig. 5. Fourier domain analysis on the temporal ciliary movement at a single location. a-d) Temporal displacement for an A-line within the ciliated area, d-i) Temporal displacement at the corresponding site, j-m) Spectrum after FFT, where the peak frequency corresponds to the CBF.

By performing the Frequency analysis on all of the locations within the ROI, the spatial CBF can be mapped out as shown by Fig. 6(a). The color bar on the top corresponds to different CBF. At each temperature, it is obvious that the CBF is mostly uniform within the patch of cilia, indicating synchronized ciliary beats. The region showing a large variance of CBF likely corresponds to asynchronized ciliary motion, which is expected to have varying frequencies. When increasing from 23 °C in Fig. 6(a) to 26 °C in Fig. 6(b), it seems that the higher temperature

Biomedical Optics EXPRESS

played a role in activating more synchronized ciliary cells. Lastly, significant increases in the CBF can be observed from the spatial maps when increasing the temperature from 23 °C to 33 °C. Figure 6(e) summarizes the mean values of the CBF, and although there are some deviations within each group, the overall trend is consistent. The histogram analysis was performed only in the area with synchronized ciliary motion. We conclude that the temperature has a positive impact on ciliary activity.

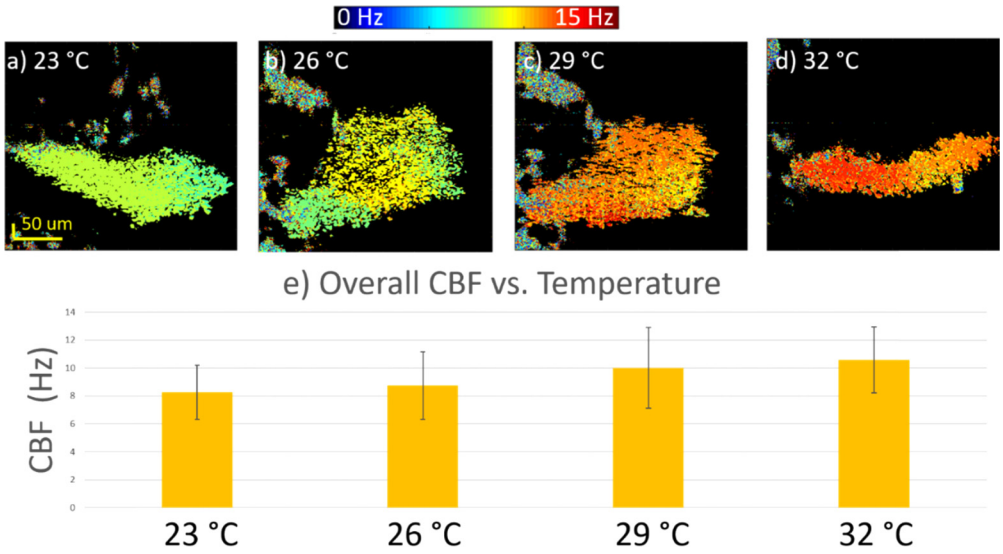

Fig. 6. Analysis of the spatial characteristics of the CBF at various temperatures. a-d) Spatial distribution of the CBF at 23 °C, 26 °C, 29 °C, and 33 °C respectively. e) Histogram of the CBF at different temperatures.

3.2. Spatially mapped CBF vs. lidocaine application

According to previous studies, lidocaine is an anesthetic that can depress the ciliary activity in the respiratory tract. Recent studies indicates that it is able to reduce the CBF, and further de-ciliated the epithelium [51]. Since the structure of the oviduct cilia is essentially identical to that of the respiratory cilia, lidocaine is expected to have a similar effect. The lidocaine experiment follows the procedure as describes in the method section, where 2% lidocaine was applied to the sample at room temperature. SEIM images were acquired at a same patch of cilia for a duration of 6.4 s before and after the lidocaine administration. By performing temporal Fourier analysis on the entire ROI, the spatial CBF maps can be generated as shown by Figs. 7(a)–7(b). Figures 7(a) and 7(b) show the spatial CBF distributions at baseline and after lidocaine administration respectively. Lidocaine application decreases the overall CBF. Additionally, the area of active cilia also decreases after lidocaine application, indicating deactivation of the ciliary cells. The results can be summarized in Fig. 6(c), which confirms the negative influence of lidocaine on ciliary activity and the feasibility of the SEIM system in detecting changes in the CBF.

Biomedical Optics EXPRESS

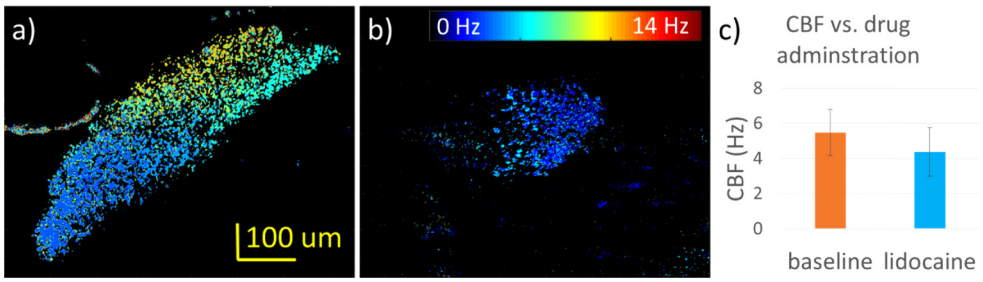

Fig. 7. Effect of 2% lidocaine administration on the CBF and the region of active cilia. a-b) Spatial CBF maps before and after lidocaine administration. c) Histogram showing the mean and standard deviation of the CBF for the control and experimental conditions.

4. Discussion and conclusion

In this study, we have developed a PRD-SS-SEIM system to image the oviduct ciliary activity in real time, as well as a Fourier domain method to analyze the spatial CBF. The system is able to resolve complete ciliary beating cycles and also allows for visualization of the synchronicity within a ciliated region. By continuously sampling the same ROI, it enables high enough sensitivity to distinguish minute CBF alterations. The feasibility of the system has been validated by imaging a porcine oviduct sample. Synchronized ciliary activity has been imaged and validated by the uniform distribution of CBF observed with the Fourier domain analysis. We have also studied the ciliary response to temperature changes and lidocaine administration. The reported outcomes correlate to that of the respiratory cilia study, where temperature and lidocaine have been shown to have a positive and negative impact respectively.

One major challenge for the clinical translation of this technology is the reduction of bulk motion during the imaging. Because the PRD method is sensitive to bulk motion, it may result in unexpected noise for the CBF measurements. One way to reduce the bulk motion is to mechanically stabilize the imaging probe using an inflatable balloon. However, contact between the balloon and tissue may affect the ciliary activity and introduce error. Since the PRD method measures the sample displacement relative to the reference reflector, we can eliminate the bulk motion in the measurement by compensating the length of the reference dynamically. In particular, we can measure the bulk motion from a non-ciliated region and use it as the reference to eliminate the bulk motion.

In this study, we have developed a novel PRD-SEIM technique to image and analyze the ciliary activity in the oviduct. The feasibility of the technique has been verified through the experiments with varying temperatures and drug administration. Compared to existing technology, the PRD-SS-SEIM system provides a more suitable FOV and the potential for ciliary endoscopy inside the fallopian tube. Although bulk motion may be an obstacle for future in-vivo studies, it can be resolved by a mechanical stabilizer and/or the use of non-ciliated region as a reference to eliminate the bulk motion. This study will serve as a stepping stone toward the clinical translation of the PRD-SS-SEIM technique to aid in the study of CBF as pertaining to infertility and abnormal pregnancies.

Funding

National Institutes of Health (P41EB-015890, R01EY-026091, R01EY-028662, R01HL-125084, R01HL-127271); Air Force Office of Scientific Research (FA9550-17-1-0193).

Biomedical Optics EXPRESS

Disclosures

Dr. Zhongping Chen has a financial interest in OCT Medical Inc., which, however, did not support this work.

References

1. M. Ezzati, O. Djahanbakhch, S. Arian, and B. R. Carr, "Tubal transport of gametes and embryos: a review of physiology and pathophysiology," J. Assist. Reprod. Genet. **31**(10), 1337–1347 (2014).
2. C. J. Pauerstein, J. D. Woodruff, and A. S. Zachary, "Factors influencing physiologic activities in the fallopian tube; the anatomy, physiology, and pharmacology of tubal transport," Obstet. Gynecol. Surv. **23**(3), 215–243 (1968).
3. H. B. Croxatto, "Physiology of gamete and embryo transport through the fallopian tube," Reprod. BioMed. Online **4**(2), 160–169 (2002).
4. Y. Ikemoto, K. Kuroda, Y. Kuribayashi, and M. Inoue, "Tubal Function Abnormalities with Tubal Patency in Unexplained Infertility," in *Treatment Strategy for Unexplained Infertility and Recurrent Miscarriage*. 2018, Springer. p. 19–31.
5. J. Kumakiri, R. Ozaki, S. Takeda, A. Malvasi, and A. Tinelli, Tubal Pregnancy, in Management and Therapy of Early Pregnancy Complications. 2016, Springer. p. 69–104.
6. S. Li and W. Winuthayanon, "Oviduct: roles in fertilization and early embryo development," J. Endocrinol. **232**(1), R1–R26 (2017).
7. R. Lyons, E. Saridogan, and O. Djahanbakhch, "The reproductive significance of human Fallopian tube cilia," Hum. Reprod. Update **12**(4), 363–372 (2006).
8. D. M. Panelli, C. H. Phillips, and P. C. Brady, "Incidence, diagnosis and management of tubal and nontubal ectopic pregnancies: a review," Fertility Research and Practice **1**(1), 15 (2015).
9. S. Halbert, P. Tam, and R. J. S. Blandau, "Egg transport in the rabbit oviduct: the roles of cilia and muscle," Science **191**(4231), 1052–1053 (1976).
10. S. A. Halbert, D. R. Becker, and S. E. Szal, "Ovum transport in the rat oviductal ampulla in the absence of muscle contractility," Biol. Reprod. **40**(6), 1131–1136 (1989).
11. W. Zhao, Q. Zhu, M. Yan, C. Li, J. Yuan, G. Qin, and J. J. C. Zhang, "Levonorgestrel decreases cilia beat frequency of human fallopian tubes and rat oviducts without changing morphological structure," Clin. Exp. Pharmacol. Physiol. **42**(2), 171–178 (2015).
12. P. Talbot, G. DiCarlantonio, M. Knoll, and C. Gomez, "Identification of cigarette smoke components that alter functioning of hamster (Mesocricetus auratus) oviducts in vitro," Biol. Reprod. **58**(4), 1047–1053 (1998).
13. D. Shi, K. Komatsu, T. Uemura, and T. Fujimori, "Analysis of ciliary beat frequency and ovum transport ability in the mouse oviduct," Genes Cells **16**(3), 282–290 (2011).
14. R. Lyons, E. Saridogan, and O. Djahanbakhch, "The effect of ovarian follicular fluid and peritoneal fluid on Fallopian tube ciliary beat frequency," Hum. Reprod. **21**(1), 52–56 (2006).
15. S. B. Liao, J. Ho, and F. J. R. Tang, "Adrenomedullin increases ciliary beat frequency and decreases muscular contraction in the rat oviduct," Reproduction (Bristol, U. K.) **141**(3), 367–372 (2011).
16. A. Bylander, M. Nutu, R. Wellander, M. Goksör, H. Billig, and D. J. J. Larsson, "Rapid effects of progesterone on ciliary beat frequency in the mouse fallopian tube," Reprod. Biol. Endocrinol. **8**(1), 48 (2010).
17. M. Knoll, R. Shaoulian, T. Magers, and P. Talbot, "Ciliary beat frequency of hamster oviducts is decreased in vitro by exposure to solutions of mainstream and sidestream cigarette smoke," Biol. Reprod. **53**(1), 29–37 (1995).
18. R. Lyons, O. Djahanbakhch, T. Mahmood, E. Saridogan, S. Sattar, M. Sheaff, A. Naftalin, and R. J. Chenoy, "Fallopian tube ciliary beat frequency in relation to the stage of menstrual cycle and anatomical site," Hum. Reprod. **17**(3), 584–588 (2002).
19. T. Nakahari, A. Nishimura, C. Shimamoto, A. Sakai, H. Kuwabara, T. Nakano, S. Tanaka, Y. Kohda, H. Matsumura, and H. Mori, "The regulation of ciliary beat frequency by ovarian steroids in the guinea pig Fallopian tube: interactions between oestradiol and progesterone," Biomed. Res. **32**(5), 321–328 (2011).
20. E. Parrilla, M. Armengot, M. Mata, J. Cortijo, J. Riera, J. L. Hueso, and D. Moratal, "Optical flow method in phase-contrast microscopy images for the diagnosis of primary ciliary dyskinesia through measurement of ciliary beat frequency. Preliminary results," in *2012 9th IEEE International Symposium on Biomedical Imaging (ISBI)*. 2012. IEEE.
21. M. Keenan, T. H. Tate, K. Kieu, J. F. Black, U. Utzinger, and J. K. Barton, "Design and characterization of a combined OCT and wide field imaging falloposcope for ovarian cancer detection," Biomed. Opt. Express **8**(1), 124–136 (2017).
22. S. Wang, J. C. Burton, R. R. Behringer, and I. V. Larina, "In vivo micro-scale tomography of ciliary behavior in the mammalian oviduct," Sci. Rep. **5**(1), 13216 (2015).
23. S. Wang and I. V. Larina, "In Vivo Imaging of the Mouse Reproductive Organs, Embryo Transfer, and Oviduct Cilia Dynamics Using Optical Coherence Tomography," in Mouse Embryogenesis. 17522018, Springer. p. 53–62.
24. S. Wang, R. Syed, O. A. Grishina, and I. V. Larina, "Prolonged in vivo functional assessment of the mouse oviduct using optical coherence tomography through a dorsal imaging window," J. Biophotonics **11**(5), e201700316 (2018).
25. G. M. Solomon, R. Francis, K. K. Chu, S. E. Birket, G. Gabriel, J. E. Trombley, K. L. Lemke, N. Klena, B. Turner, and G. J. Tearney, "Assessment of ciliary phenotype in primary ciliary dyskinesia by micro-optical coherence tomography," JCI insight **2**(5), e91702 (2017).

Biomedical Optics EXPRESS

26. D. Cui, K. K. Chu, B. Yin, T. N. Ford, C. Hyun, H. M. Leung, J. A. Gardecki, G. M. Solomon, S. E. Birket, and L. Liu, "Flexible, high-resolution micro-optical coherence tomography endobronchial probe toward in vivo imaging of cilia," Opt. Lett. **42**(4), 867–870 (2017).
27. J. C. Jing, J. J. Chen, L. Chou, B. J. Wong, and Z. Chen, "Visualization and detection of ciliary beating pattern and frequency in the upper airway using phase resolved Doppler optical coherence tomography," Sci. Rep. **7**(1), 8522 (2017).
28. B. T. Lemieux, J. J. Chen, J. Jing, Z. Chen, and B. J. Wong, "Measurement of ciliary beat frequency using Doppler optical coherence tomography," in International forum of allergy & rhinology. 2015. Wiley Online Library.
29. Z. Chen, T. E. Milner, S. Srinivas, X. Wang, A. Malekafzali, M. J. van Gemert, and J. S. Nelson, "Noninvasive imaging of in vivo blood flow velocity using optical Doppler tomography," Opt. Lett. **22**(14), 1119–1121 (1997).
30. Y. Zhao, Z. Chen, C. Saxer, S. Xiang, J. F. de Boer, and J. S. Nelson, "Phase-resolved optical coherence tomography and optical Doppler tomography for imaging blood flow in human skin with fast scanning speed and high velocity sensitivity," Opt. Lett. **25**(2), 114–116 (2000).
31. Y. He, Y. Qu, J. Zhu, Y. Zhang, A. Saidi, T. Ma, Q. Zhou, and Z. Chen, "Confocal Shear Wave Acoustic Radiation Force Optical Coherence Elastography for Imaging and Quantification of theIn VivoPosterior Eye," IEEE J. Sel. Top. Quantum Electron. **25**(1), 1–7 (2019).
32. Y. Qu, Y. He, A. Saidi, Y. Xin, Y. Zhou, J. Zhu, T. Ma, R. H. Silverman, D. S. Minckler, and Q. Zhou, "In vivo elasticity mapping of posterior ocular layers using acoustic radiation force optical coherence elastography," Invest. Ophthalmol. Visual Sci. **59**(1), 455–461 (2018).
33. Y. Qu, Y. He, Y. Zhang, T. Ma, J. Zhu, Y. Miao, C. Dai, M. Humayun, Q. Zhou, and Z. Chen, "Quantified elasticity mapping of retinal layers using synchronized acoustic radiation force optical coherence elastography," Biomed. Opt. Express **9**(9), 4054–4063 (2018).
34. J. Zhu, L. Qi, Y. Miao, T. Ma, C. Dai, Y. Qu, Y. He, Y. Gao, Q. Zhou, and Z. Chen, "3D mapping of elastic modulus using shear wave optical micro-elastography," Sci. Rep. **6**(1), 35499 (2016).
35. J. Zhu, Y. Miao, L. Qi, Y. Qu, Y. He, Q. Yang, and Z. Chen, "Longitudinal shear wave imaging for elasticity mapping using optical coherence elastography," Appl. Phys. Lett. **110**(20), 201101 (2017).
36. Y. Qu, T. Ma, Y. He, J. Zhu, C. Dai, M. Yu, S. Huang, F. Lu, K. K. Shung, and Q. Zhou, "Acoustic radiation force optical coherence elastography of corneal tissue," IEEE J. Sel. Top. Quantum Electron. **22**(3), 288–294 (2016).
37. J. Zhu, J. Yu, Y. Qu, Y. He, Y. Li, Q. Yang, T. Huo, X. He, and Z. Chen, "Coaxial excitation longitudinal shear wave measurement for quantitative elasticity assessment using phase-resolved optical coherence elastography," Opt. Lett. **43**(10), 2388–2391 (2018).
38. G. Tearney, M. Shishkov, and B. E. Bouma, "Spectrally encoded miniature endoscopy," Opt. Lett. **27**(6), 412–414 (2002).
39. G. J. Tearney, R. Webb, and B. E. Bouma, "Spectrally encoded confocal microscopy," Opt. Lett. **23**(15), 1152–1154 (1998).
40. M. Ikuta, D. Do, D. Kang, G. J. Tearney, and J. S. Brauer, Spectrally encoded endoscopic probe having a fixed fiber, in, Editor Editors. 2017, Google Patents. p.
41. Z. Chen, T. E. Milner, D. Dave, and J. S. Nelson, "Optical Doppler tomographic imaging of fluid flow velocity in highly scattering media," Opt. Lett. **22**(1), 64–66 (1997).
42. S. Grechin and D. Yelin, "Imaging acoustic vibrations in an ear model using spectrally encoded interferometry," Opt. Commun. **407**, 175–180 (2018).
43. O. Ilgayev and D. Yelin, "Phase-sensitive imaging of tissue acoustic vibrations using spectrally encoded interferometry," Opt. Express **21**(17), 19681–19689 (2013).
44. D. Yelin, B. Bouma, J. Rosowsky, and G. Tearney, "Doppler imaging using spectrally-encoded endoscopy," Opt. Express **16**(19), 14836–14844 (2008).
45. S. Yun, G. Tearney, J. de Boer, and B. Bouma, "Pulsed-source and swept-source spectral-domain optical coherence tomography with reduced motion artifacts," Opt. Express **12**(23), 5614–5624 (2004).
46. J. Walther, G. Mueller, H. Morawietz, and E. Koch, "Signal power decrease due to fringe washout as an extension of the limited Doppler flow measurement range in spectral domain optical coherence tomography," J. Biomed. Opt. **15**(4), 041511 (2010).
47. J. F. De Boer, R. Leitgeb, and M. Wojtkowski, "Twenty-five years of optical coherence tomography: the paradigm shift in sensitivity and speed provided by Fourier domain OCT," Biomed. Opt. Express **8**(7), 3248–3280 (2017).
48. M. A. Choma, M. V. Sarunic, C. Yang, and J. A. Izatt, "Sensitivity advantage of swept source and Fourier domain optical coherence tomography," Opt. Express **11**(18), 2183–2189 (2003).
49. S.-H. Yun, G. J. Tearney, J. F. de Boer, N. Iftimia, and B. E. Bouma, "High-speed optical frequency-domain imaging," Opt. Express **11**(22), 2953–2963 (2003).
50. J. Zhang, B. Rao, L. Yu, and Z. Chen, "High-dynamic-range quantitative phase imaging with spectral domain phase microscopy," Opt. Lett. **34**(21), 3442–3444 (2009).
51. K. J. Ingels, M. R. Nijziel, K. Graamans, and E. H. Huizing, "Influence of cocaine and lidocaine on human nasal cilia: beat frequency and harmony in vitro," Arch. Otolaryngol., Head Neck Surg. **120**(2), 197–201 (1994).